





Modelling power-law ultrasound absorption using a time-fractional, static memory, Fourier pseudo-spectral method

Matthew J. King,^{1,a)}  Timon S. Gutleb,²  B. E. Treeby,¹  and B. T. Cox¹ 

¹Department of Medical Physics and Biomedical Engineering, University College London, London, WC1E 6BT, United Kingdom

²School of Computer Science, University of Leeds, Leeds, LS2 9JT, United Kingdom

ABSTRACT:

We describe and implement a numerical method for modelling the frequency-dependent power-law absorption of ultrasound in tissue, as governed by the first order linear wave equations with a loss taking the form of a fractional time derivative. The (Caputo) fractional time derivative requires the full problem history, which is contained within an iterative procedure. The resulting numerical method requires a fixed (static) memory cost, irrespective of the number of time steps. The spatial domain is treated by the Fourier spectral method. Numerically, comparisons are made against a model for the same power-law absorption with loss described by the fractional-Laplacian operator. One advantage of the fractional time derivative over the fractional-Laplacian operator is the local treatment of the power-law, allowing for a spatially varying frequency power-law. © 2025 Acoustical Society of America.

<https://doi.org/10.1121/10.0035937>

(Received 7 August 2024; revised 8 January 2025; accepted 2 February 2025; published online 13 March 2025)

[Editor: James F. Lynch]

Pages: 1761–1771

I. INTRODUCTION

The rate of absorption of ultrasound waves in the body depends on frequency and, for the range of frequencies of interest for biomedical ultrasound, typically follows a power-law (Wells, 1975; Narayana and Ophir, 1983; Goss *et al.*, 1979; Treeby and Cox, 2010b). The absorption coefficient is, therefore, commonly written in the form $\alpha = \alpha_0 \omega^y$, where ω is the temporal frequency and α_0 and y are tissue-dependent parameters (Szabo, 1994; Chen and Holm, 2004). Lossy wave equations that account for frequency-dependent absorption were first derived for integer values of the exponent, y (Blackstock, 1967; Stokes, 2007). However, for most biological tissues, y is a non-integer lying in the range $0 < y < 2$ (Li *et al.*, 2022). Wave equations exhibiting this behaviour have been developed using fractional time derivative operators (Caputo, 1967; Szabo, 1994; Liebler *et al.*, 2004; Wismer, 2006). A consequence of the use of a time-fractional derivative on numerical approaches to solving these equations is the need to store some history of the wavefield, and hence, the need for additional computational memory. The amount of additional memory required grows significantly as y approaches 1. To avoid this memory issue, a fractional-Laplacian has been used in place of a fractional time derivative (Chen and Holm, 2003; Treeby and Cox, 2010b). This can be straightforwardly computed within the context of pseudo-spectral models using the fast Fourier transform (FFT) without the need to store the history of the wavefield. This is the approach taken in the software package, *k-Wave* (see <http://www.k-wave.org>) (Treeby and Cox, 2010a). However, there are drawbacks. First, the power-law

that is modelled is not strictly a power-law of the frequency, ω^y , as would be observed in experiments, but of the wave-number k^y , which for ω to follow the power law relies on close adherence to the loss-less dispersion relation $\omega = c_0 k$. Second, the power-law exponent y —because it is implemented in k -space—cannot be spatially varying. To allow heterogeneous power-law absorption to be modelled accurately, this paper focuses on the equations that use fractional time derivatives and looks at alternative methods of tackling the memory problem.

Several alternative approaches for resolving the increased memory requirement of time-fractional derivative methods have been suggested, including the fixed memory principle (Podlubny, 1998) and the logarithmic memory principle (Ford and Simpson, 2001), as well as methods (Yuan and Agrawal, 2002; Diethelm, 2008; Birk and Song, 2010) that re-frame the integral into a double integral form, accounting for the full history with an iterative procedure and quadrature rule. The specific procedure used here is of this latter type, adapted from the work of Birk and Song (2010). This method is also discussed and a range of numerical examples are given in Gutleb and Carrillo (2023), which highlights specific implementation approaches that we adapt to make use of the k -space pseudo-spectral method and minimise the additional memory costs of the approach. Gutleb and Carrillo (2023) additionally discuss the potential for the time-fractional derivative given being used on lossy wave equation given by Caputo/Wismer, citing this as their primary motivation. However, they actually make use of the form given by Szabo (1994). This is performed on a two-dimensional (2D) disk in line with the majority of Gutleb and Carrillo (2023) focusing on a spectral approach in order to resolve the problems in a wider range of spatial domains.

^{a)}Email: matthew.king@ucl.ac.uk

This work is divided into two main sections. Section II gives the theoretical background, the governing equations and each of their parameters, along with a breakdown of the static memory method for the fractional time derivative. It concludes with a discussion of the numerical scheme used for the evaluation of the fractional time derivatives. In Sec. III, a number of numerical results are presented illustrating the convergence of the static memory method in each of its parameters with comparisons to the fractional-Laplacian approach (as implemented in *k*-Wave). This is followed by the illustration of the ability of the time-fractional method to correctly predict the absorption through a one-dimensional (1D) example. Section III concludes by considering examples with heterogeneous y in both 1D and three-dimensional (3D), making comparisons to a homogenised *k*-Wave formulation.

II. THEORY

A. Governing equations

One way to model power-law absorption of acoustic pressure waves is through a wave equation with a loss term described, as in the Caputo/Wisner equations, by the fractional time derivative of the Laplacian of the pressure, p ,

$$\frac{1}{c_0^2} \frac{\partial^2 p}{\partial t^2} = \nabla^2 p + \tau \frac{\partial^{y-1}}{\partial t^{y-1}} \nabla^2 p, \quad (1)$$

where c_0 is the sound speed and τ is related to the absorption coefficient. However, instead of solving this equation directly, we will instead make use of the equivalent system of first order equations

$$\rho_0 \frac{\partial \mathbf{u}}{\partial t} = -\nabla p, \quad (2a)$$

$$\frac{\partial \rho}{\partial t} = -\rho_0 \nabla \cdot \mathbf{u}, \quad (2b)$$

$$p = c_0^2 \left(\rho + \tau \frac{\partial^{y-1} \rho}{\partial t^{y-1}} \right). \quad (2c)$$

The introduction of the time-fractional derivative in the acoustic equation of state [Eq. (2c)] may be viewed as accounting for the material properties, and can be interpreted physically in terms of springs and dampers (Mainardi, 2022). By taking the second time derivative of Eq. (2c), it is easy to show that these equations give rise to Eq. (1). An expression for τ in terms of the absorption coefficient can be found by considering the propagation of the plane wave

$$p = p_0 \exp^{i(kx - \omega t)}. \quad (3)$$

We note that the wave will only attenuate for a real frequency, ω , when the wavenumber $k = k_r + ik_i$ has a positive imaginary part, with the decay rate k_i . Since we are

modelling power-law absorption following $\alpha = \alpha_0 \omega^y$, we set $k_i = \alpha$. Expanding Eq. (1) with Eq. (3), gives

$$k_i^2 = \frac{1}{2} \frac{\omega^2}{c_0^2} \frac{-\left(1 + \tau \omega^{y-1} \cos\left(\frac{-\pi(y-1)}{2}\right)\right)}{1 + 2\tau \omega^{y-1} \cos\left(\frac{-\pi(y-1)}{2}\right) + (\tau \omega^{y-1})^2} \pm \frac{\sqrt{1 + 2\tau \omega^{y-1} \cos\left(\frac{-\pi(y-1)}{2}\right) + (\tau \omega^{y-1})^2}}{1 + 2\tau \omega^{y-1} \cos\left(\frac{-\pi(y-1)}{2}\right) + (\tau \omega^{y-1})^2}. \quad (4)$$

While the above expression is exact, if we additionally assume that $\tau \omega^{y-1} \ll 1$, the resulting asymptotic expression for k_i is given as

$$k_i = \tau \frac{\sin\left(\frac{\pi(y-1)}{2}\right)}{2c_0} \omega^y + O((\tau \omega^{y-1})^3), \quad (5)$$

and so, in terms of the absorption parameters, setting $k_i = \alpha_0 \omega^y$,

$$\tau = \frac{2c_0 \alpha_0}{\sin\left(\frac{\pi(y-1)}{2}\right)}. \quad (6)$$

(For an extended derivation, see the supplementary material.)

B. Static memory fractional time derivative

This section summarises the theories of Birk and Song (2010) and Gutleb and Carrillo (2023), describing the method used to approximate the fractional time derivative. We begin by considering the Caputo fractional derivative of order Y (Caputo, 1966) as given by

$$\frac{\partial^Y f}{\partial t^Y}(t) = \frac{1}{\Gamma([Y] - Y)} \int_0^t \frac{f^{[Y]}(\tilde{t})}{(t - \tilde{t})^{Y+1-[Y]}} d\tilde{t} \quad (7a)$$

$$= \frac{1}{\Gamma(1 - Y)} \int_0^t \frac{f'(\tilde{t})}{(t - \tilde{t})^Y} d\tilde{t}, \quad (7b)$$

where the latter equation arises because, in this work, we will only be concerned with $y = Y + 1 \in (1, 2)$, i.e., $Y \in (0, 1)$, and so $[Y] = 1$. $f'(t)$ denotes the ordinary derivative with respect to t . In order to evaluate this integral, we can expand the Gamma function into an integral between $(0, \infty)$ and apply a change of basis. This is detailed in the supplementary material:

$$\frac{\partial^Y f}{\partial t^Y}(t) = \int_0^\infty \frac{2 \sin(\pi \alpha)}{\pi} s^{2Y-1} \phi_f(s, t) ds, \quad (8a)$$

$$\phi_f(s, t) = \int_0^t e^{-s^2(t-\tilde{t})} f'(\tilde{t}) d\tilde{t}. \quad (8b)$$

We proceed by evaluating the outer integral between $(0, \infty)$ through a quadrature rule, writing the problem as

$$\frac{\partial^Y f}{\partial t^Y}(t) = \sum_{j=1}^L A_j \int_0^t e^{-s_j^2(t-\tilde{t})} f'(\tilde{t}) d\tilde{t}. \quad (9)$$

To do this, we will make use of the Gauss–Jacobi quadrature points, x_j , and weights, λ_j , for the interval $(-1, 1)$, which results in Eq. (8) being expressed as

$$\frac{\partial^Y f}{\partial t^Y}(t) = \sum_{j=0}^L \lambda_j \frac{8 \sin(\pi\alpha)}{\pi(1+x_j)^4} \phi_f\left(\frac{(1+x_j)^2}{(1-x_j)^2}, t\right), \quad (10a)$$

$$\frac{\partial^Y f}{\partial t^Y}(t) = \sum_{j=0}^L A_j \phi_f(s_j, t) \quad (10b)$$

with

$$A_j = \lambda_j \frac{8 \sin(\pi\alpha)}{\pi(1+x_j)^4}, \quad s_j = \frac{(1+x_j)^2}{(1-x_j)^2}. \quad (10c)$$

We refer to s_j and A_j as the Birk–Song quadrature points and weights, respectively, as described in [Birk and Song \(2010\)](#). L is a free parameter dictating the number of quadrature points used. This process can be repeated for $Y > 1$, adjusting Eq. (8) as given in [Birk and Song \(2010\)](#) and [Gutleb and Carrillo \(2023\)](#). Alternatives to the Birk–Song points are also available, such as those given in [Diethelm \(2008\)](#) and [Yuan and Agrawal \(2002\)](#).

The advantage of writing the time-fractional derivative as a sum of integrals is that ϕ_f lends itself easily to being updated in discrete time steps. Set

$$\phi_f(s_j, t) = \psi_j(t) = \int_0^t e^{-s_j^2(t-\tilde{t})} f'(\tilde{t}) d\tilde{t}, \quad (11)$$

$$\psi_j(t + \delta t) = e^{-s_j^2 \delta t} \psi_j(t) + \int_t^{t+\delta t} e^{-s_j^2(t+\delta t-\tilde{t})} f'(\tilde{t}) d\tilde{t}. \quad (12)$$

For suitably small δt , it is then possible to approximate $f'(\tilde{t})$ through interpolation, allowing the integral to be expressed in a closed form, which is exact for this interpolation. Assuming $f(t)$ is piecewise linear on intervals $(n\delta t, (n+1)\delta t)$, it follows that

$$\begin{aligned} \psi_j((n+1)\delta t) &= e^{-s_j^2 \delta t} \psi_j(n\delta t) \\ &+ \frac{1 - e^{-s_j^2 \delta t} f((n+1)\delta t) - f(n\delta t)}{s_j^2 \delta t}. \end{aligned} \quad (13)$$

This has an error of order $O(N\delta t)$ after N time steps in each of the ψ_j . Taking higher order interpolating polynomials also yields exact forms through integration by parts. This is

detailed in the supplementary material, though not used here due to the time step sizes considered.

C. Numerical scheme

Here, we describe a numerical procedure for evaluating Eq. (2) in one dimension, using τ given by Eq. (6) and evaluating the time-fractional derivative by Eq. (9).¹ With the FFT denoted \mathbb{F} and inverted by \mathbb{F}^{-1} . Additionally,

$$u^n = u((n-1/2)\delta t, \mathbf{x}), \quad (14a)$$

$$\rho^n = \rho(n\delta t, \mathbf{x}), \quad (14b)$$

$$p^n = p(n\delta t, \mathbf{x}), \quad (14c)$$

$$\psi_j^n = \psi_j(n\delta t, \mathbf{x}), \quad (14d)$$

where each variable is represented as an array of the size of the spatial grid corresponding to \mathbf{x} . (Note that the ψ_j^n are L such variables of spatial grid size, as indexed by j .) The update equations for acoustic particle velocity and pressure can be written as

$$u^n = u^{n-1} - \frac{\delta t}{\rho_0} \mathbb{F}^{-1}(ik\kappa \mathbb{F}(p^n)), \quad (15a)$$

$$\rho^n = \rho^{n-1} - \delta t \mathbb{F}^{-1}(ik\kappa \mathbb{F}(\rho_0 u^n)), \quad (15b)$$

where κ is a k -space correction to reduce numerical dispersion ([Treeby and Cox, 2010a](#)). Noting that τ , A_j , and s_j can be pre-computed using Eqs. (6) and (10c), we then update the values of $\psi_j(n\delta t, \mathbf{x})$ of ρ following Eq. (13),

$$\psi_j^n = e^{-s_j^2 \delta t} \psi_j^{n-1} + \frac{1 - e^{-s_j^2 \delta t}}{s_j^2} \frac{\rho^n - \rho^{n-1}}{\delta t}. \quad (16)$$

Instead of the forward difference approximation, we could have used the gradient as already computed using the FFT for Eq. (15b). While for this specific case, the result would be more accurate, removing any cancellation errors, when a perfectly matched layer (PML) is used, this results in a reduced accuracy if not accounted for in the ψ_j correctly. Since in these cases $\rho(n\delta t)$ has already been computed, and the cost for storing $\rho((n-1)\delta t)$ is fixed, we choose to use the form given by Eq. (16). Additionally, using the forward difference approximation allows for the inclusion of additive sources, which are added after the FFTs have been applied. Now, we are ready to close the system by computing p^n ,

$$p^n = c_0^2 \left(\rho^n + \tau \sum_{j=1}^L A_j \psi_j \right), \quad (17)$$

where \cdot_j represents the vector dot product in j at each point in the grid. As previously mentioned, in the numerical results provided below, we have additionally included a PML to prevent wave wrapping within the domain, which is assumed to be periodic due to the use of the FFT. This

change only impacts Eq. (15) and is detailed within the literature, such as in [Tabei et al. \(2002\)](#) and [Treeby and Cox \(2010a,b\)](#).

III. NUMERICAL EXPERIMENTS

Here, the numerical scheme consisting of Eqs. (15)–(17) will be demonstrated with examples.² First, we will examine the accuracy of the time-fractional numerical scheme as L and δt are varied. For the variation of δt , we make use of the Courant–Friedrichs–Lewy (CFL) ([Courant et al., 1967](#)) number for 1D, acting as a normalised time step given by $CFL = c_0 \delta t / \delta x$. As such, increasing or decreasing the CFL is equivalent to increasing or decreasing δt , respectively. (With c_0 and δx remaining fixed.) Traditionally, the CFL number is used to ensure stability, with an explicit time solver as we have here, being stable for $CFL < 1$. In higher dimensions, the formulation sums the above expression across each of the dimensions; however, for simplicity, the number we give here will always be given only by the first dimension.

Second, the absorption power-laws that result from the scheme are compared to those that use the fraction Laplacian, as implemented in k -Wave. Finally, 1D and 3D examples are given in which the absorption power-law exponent, y , varies throughout the domain. Throughout this section, we make use of the parameters given in Table I, unless stated otherwise in the figure captions.

A. Convergence in L and δt

For Figs. 1 and 2, three different power-laws, $\alpha = \alpha_0 \omega^y$, and three different timesteps, δt (through the CFL) are considered. The problem, a 1D simulation across 16 mm with a point source located 4 mm into the domain, is run over 7 μ s with a sensor located 10 mm from a point pressure source. The errors considered are those in the sensor signal. In Fig. 1, this is done sequentially, comparing the signals for each fixed value to L to the signal for $L=10$, with Fig. 1 plotting the error in the l^∞ norm with the l^2 norm behaving similarly.

Figure 2 instead compares the signals to a reference produced by running the same simulation with a CFL of

6.25×10^{-4} and $L = 300$. In order to compare the reference signal to the sensor signals, the reference signal is sampled at the times for which the sensor records a point.

In Fig. 1, it can be observed that, irrespective of the time step size, the improvement in the sensor output is uniform between the case for increasing values of L . This remains true even for different values of y with each case also giving similar results. Despite the consistent convergence in L for any given CFL, this does not mean we are converging to an exact solution, rather for large enough L , the error from the choice of δt becomes dominant. As a result, for each δt , we converge to a solution with a minimum fixed error in L . This same behaviour was observed in [Gutleb and Carrillo \(2023\)](#) for the approximation of the fractional derivative. This is most clearly seen here in Fig. 2 where for each of the CFL considered, increasing L decreases the error only so far before it plateaus and becomes approximately constant. For a decreased CFL, and therefore smaller time step δt , it may be observed that a higher value of L is required to reach this plateau; however, for each fixed L , decreasing the time step results in a smaller error.

While it can be observed that each of the three y values produce the similar error, irrespective of the choice of the CFL for large y , in Fig. 2, we may observe that the rate at which the error plateaus is different, becoming steady for a smaller value of L for y closer to 2, suggesting that for the larger values of y the error for a fixed δt is larger compared to the error from the choice of L , and therefore dominates. This is more clearly seen in Fig. 3 where a fixed α_0 and varied y , and a fixed y and varied α_0 are considered.

In Fig. 3 (left), it can be observed that, when just y is varied, most of the behaviour of Fig. 2 (bottom right) is still captured—with the larger values of y producing smaller errors for the same value of L until the error plateaus. In Fig. 3 (right), on the other hand, the three different values of α_0 present very little variation, showing the exact same behaviour across the different CFL and L values. While the larger values for α_0 do perform marginally better across the cases, this difference is not comparable to the differences observed in Fig. 2.

Rather than comparing the time-fractional solution to itself, we can also compare against the Green's function solution to the second order PDE problem.¹ Approximate methods for computing the Green's function are given in, for example, [Kelly and McGough \(2016\)](#). Alternatively, we can make use of the exact Green's function solution given in [Treeby and Cox \(2011\)](#), which instead of the time-fractional derivative term gives the loss in terms of the fractional-Laplacian. It should be noted that the two problems are equivalent up to the order of perturbation within the linearised Euler equations with loss. The advantage of using the Green's function solutions is that they are exact when considered in homogeneous domains. While the Green's function solution cannot be extended to the heterogeneous model, when considered in a homogeneous domain, it provides a suitable test case, capturing the correct absorption

TABLE I. Typical parameters for c_0 , $\alpha = \alpha_0 \omega^y$, and ρ_0 . Figures 1–9 used (a)–(c) and the named tissues were used for Fig. 10. The data are taken from [Treeby and Cox, J. Acoust. Soc. Am. 127\(5\), 2741–2748 \(2010b\)](#); [Lou et al., J. Biomed. Opt. 22\(4\), 041015 \(2017\)](#); [Szabo, Diagnostic Ultrasound Imaging: Inside Out, Academic Press, 2004, Table B.1.](#); and [Moran et al., Ultrasound Med. Biol. 21\(9\), 1177–1190 \(1995\)](#).

	c_0	α_0	y	ρ_0	Cite
(a)	1500	0.5	1.1	1	Treeby and Cox (2010b)
(b)	1500	0.25	1.5	1	Treeby and Cox (2010b)
(c)	1500	0.1	1.9	1	Treeby and Cox (2010b)
Fat	1470	0.6	1.01	937	Lou et al. (2017) ; Szabo (2014)
Blood vessel	1584	0.14	1.21	1040	Lou et al. (2017) ; Szabo (2014)
Skin	1650	0.22	1.15	1150	Lou et al. (2017) ; Moran et al. (1995)
Fibroglandular	1515	0.75	1.5	1040	Lou et al. (2017) ; Szabo (2014)

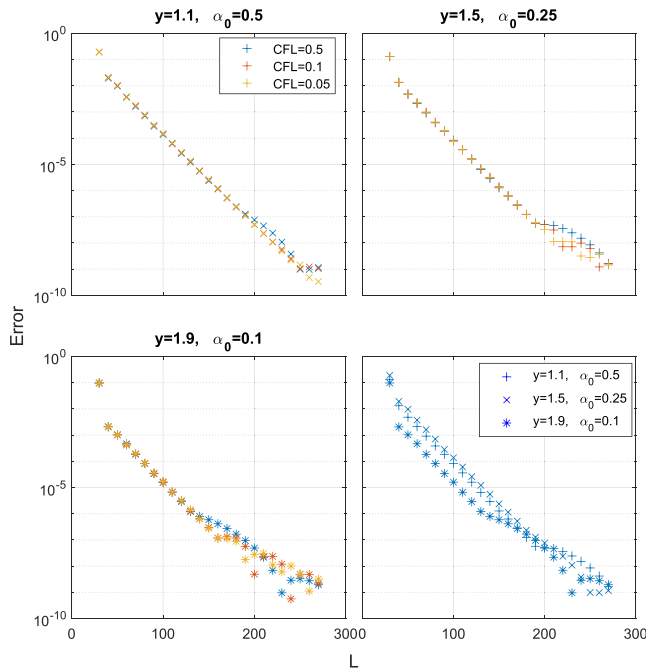


FIG. 1. Normalised maximum error, L^∞ , of the pressure at the sensor between $p(t, L)$ and $p(t, L-10)$. Plotted for parameter sets (a)–(c) as indicated according to Table I with CFL = 0.5, 0.1, and 0.05, and for CFL = 0.5 for each parameter set (bottom right).

behaviour. Additionally, we may compare the rates of convergence between the fractional-Laplacian loss, and the time-fractional approach to the Green's function, which is included in the *k*-Wave MATLAB package (Mathworks Inc., Natick, MA) (Treeby and Cox, 2011).

Plotted in Fig. 4 are the normalised errors for the first order ordinary differential equation (ODE) solver, with loss described both by the fractional-Laplacian and the time-fractional derivative as discussed here, with $L = 80$. These are compared to the second order ODE Green's function for the fractional-Laplacian loss. The choice of L is due to the near-convergence seen for each of the CFL numbers in Figs. 2 and 3, with the error dictated by choice of the CFL and not the quadrature rule, except for exceptionally small time steps. Improved errors may be observed for the smaller CFL numbers by increasing L further. This choice of L additionally limits the increased computational cost of the method, both in memory storage, and number of operations compared to the fractional-Laplacian method, with L increasing these both linearly. This is detailed further in Sec. IV.

For all three of the parameter pairs for α , it may be observed that both methods converge to the Green's function solution as would be expected, confirming that in the small δt limit, the two methods are equivalent, further validating the time-fractional method as an alternative approach to modelling power-law absorption to the traditional fractional-Laplacian method. In addition to this, it is interesting to notice that despite representing a different loss term, the model that uses the time-fractional derivative converges faster than the fractional-Laplacian model to the Green's function solution with fractional-

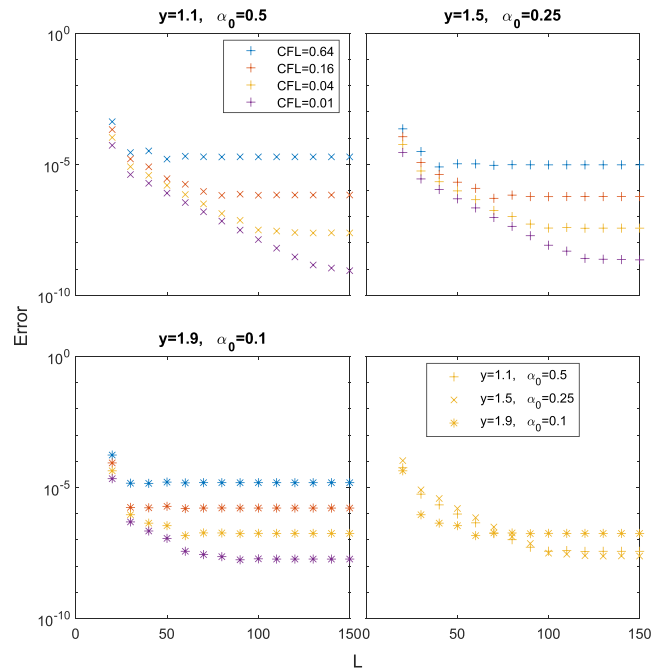


FIG. 2. As shown in Fig. 1, comparing $p(t, L)$ with the indicated CFL numbers to $p(t, 300)$ with a CFL of 6.25×10^{-4} . Plotted with CFL = 0.64, 0.16, 0.04, and 0.01 and for CFL = 0.04 for each y (bottom right).

Laplacian loss. In particular, between $CFL = 2^{-3}$ and 2^{-9} , in the case of $y = 1.1$ and $\alpha_0 = 0.5$, the time-fractional method produces an error of the same magnitude as the fractional-Laplacian with a CFL 2^{-4} smaller, i.e., the same accuracy is being retrieved for a time step that is 16 times larger. For the values $y = 1.5$ and $\alpha_0 = 0.25$, this is

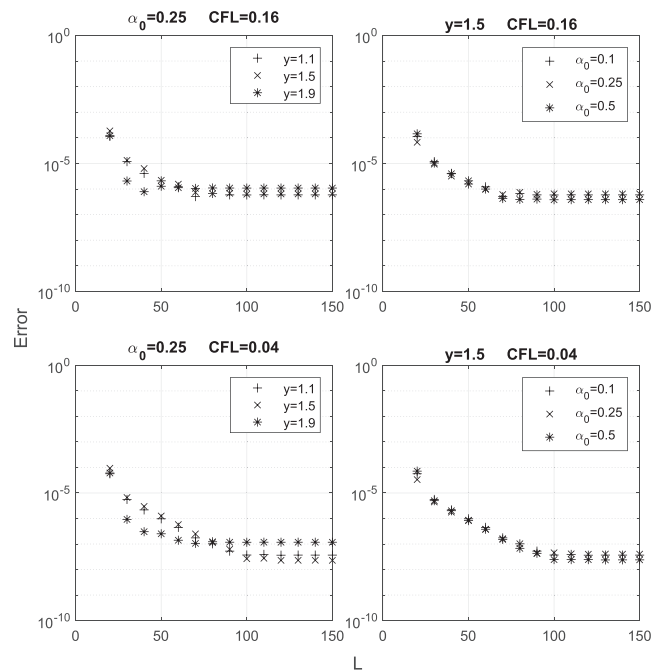


FIG. 3. As shown in Fig. 2, comparing $p(t, L)$ with the indicated CFL numbers to $p(t, 300)$ with a CFL of 6.25×10^{-4} . Plotted with CFL = 0.16 (top) and CFL = 0.04 (bottom) we vary y for a fixed $\alpha_0 = 0.25$ (left), and vary α_0 for a fixed $y = 1.5$ (right).

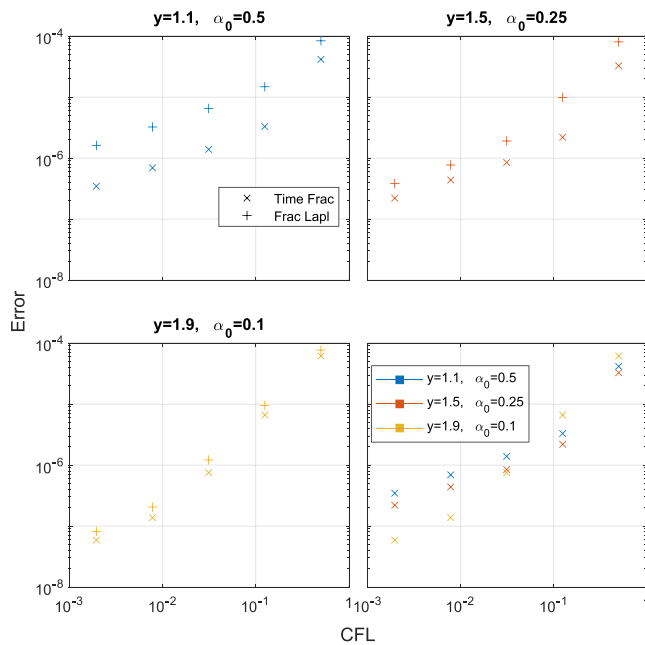


FIG. 4. Comparison between the reference Green's function solution for the fractional-Laplacian loss and the solution from the first order equations with the time-fractional loss term ($L=80$, \times) and with the fractional-Laplacian loss ($+$). Errors computed for CFL numbers between 2^{-1} and 2^{-9} . The errors have been normalised against the maximum value of the second order solution at the sensor location. Pairs of α_0 and y are as used in Fig. 1, with the bottom right plot only showing the results for the time-fractional derivative for each power-law considered.

reduced to only four times larger, and in the final case, only observes a small improvement. However, noting that for soft tissues y is typically close to 1 implies that the improvement seen in the first case could represent a significant computational saving by considering the time-fractional approach. Observing the bottom right plot of Fig. 4, which plots all three cases just for the fractional-Laplacian method, as the CFL decreases, the error decreases at a faster rate in y . This coincides with the reduced difference between the time-fractional and fractional-Laplacian methods, which already allows for a larger time step.

B. Absorption

We now test how well the method reproduces each $\alpha(\omega)$ by comparing the observed absorption to the frequency-dependant power-law given by the input parameters. In addition to this, we make use of the Kramers–Kronig relation (Waters *et al.*, 2005; Waters *et al.*, 2000) to compare the observed dispersive wave speed to predicted values for the given power-law. This is done as in Treeby and Cox (2010b) for the loss generated by the fractional-Laplacian, which we will additionally compare against. Each of the figures in this section have been produced considering the following simulation: a 1D, 12.2 mm domain is considered under a uniform spatial grid of size 1024, over a time of 4 μ s for a CFL of 0.05. A point pressure source applied at time, $t=0$, is located 3.05 mm into the domain, with two

sensors located 3.55 and 4.55 mm in the domain. The sensor data are recorded and their respective amplitude and phase spectra are found. This information is then processed into the absorption by comparing the amplitude spectrum of the two sensors, and the dispersion through the phase spectrum. Figures 5 and 6 plot α and C_p for four values of L . These are $L=20$, $L=40$, $L=80$, and $L=160$.

For $L=20$, it is clear that the simulation has failed to predict the absorption correctly, with no frequency dependence observed, but rather a constant value of α . This problem is mostly resolved for $L=40$; however, each case observes divergence between the prediction and simulations as the frequency increases. Increasing to $L=80$ reduces the error for all three with only small differences between the cases of $L=80$ and $L=160$. This is similarly observed for the dispersion, with $L=20$ unable to correct predict c_p , while $L=40$ reproduces the prediction for low frequencies but then breaks down for the higher frequencies. Similar results are produced by $L=80$ and $L=160$; however, for $y=1.9$, the higher frequencies still observe this difference. This may be anticipated through Fig. 2 where, in the bottom right plot, we compare the errors for the three values of y . Here, we observe that, while for $y=1.9$ we see convergence in L faster than for the lower values of y , it is observable that these lower values actually produce a smaller error for a CFL of 0.04, which is comparable to that used for this simulation.

It is natural to then compare these results to those produced for the fractional-Laplacian using the *k*-Wave toolbox; this is performed in Fig. 7. Here, we have chosen $L=120$.

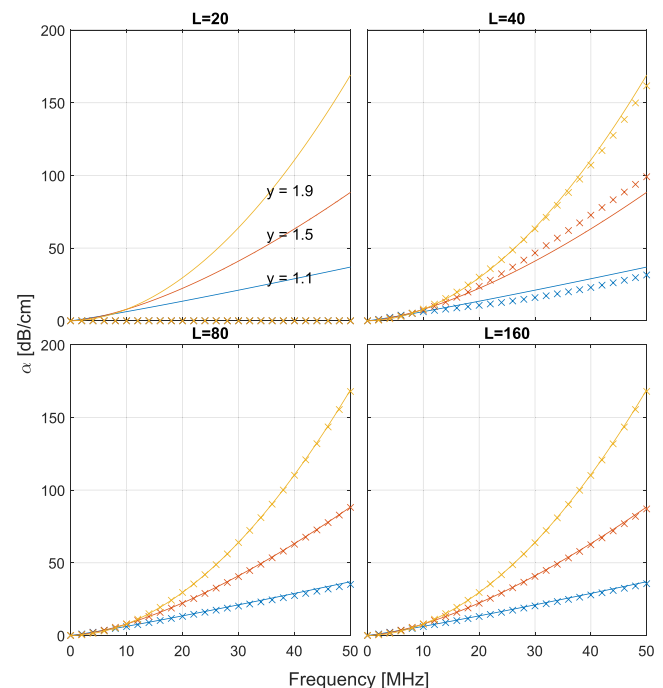


FIG. 5. Absorption α for $L=20$, 40, 80, and 160 computed as described in the main text. Solid lines describe the predicted absorption while circles mark on the values found through the simulation. For $L=20$ (top left), the results from the predicted absorption are indistinguishable between the three cases.

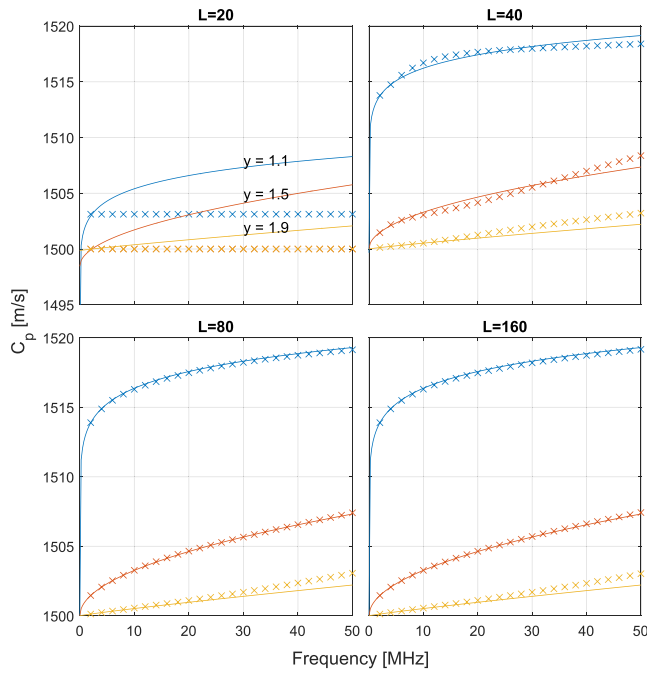


FIG. 6. As shown in Fig. 5 but showing the dispersion. Both predicted (solid lines) and from the simulation.

In this figure, it can be observed for each of the values of y that the results produced are very similar between the two methods. However, it may be observed in the dispersion for $y = 1.5$ and $y = 1.9$, where the time-fractional derivative was least accurate to the predictions, that this method performs better than when the loss is given by the fractional-Laplacian. This improvement from the fractional-Laplacian to the time-fractional derivative may have been anticipated from Fig. 4 where this improvement was observed for each parameter set considered. Observing the plot of the dispersive sound speed, it may be suggested that the larger values of y present a larger error, suggesting a contradiction to the results of Fig. 4. There are two important features to note: first, the waves with the highest frequency will decay fastest, which is where this error is observed most readily, minimising the effect of these high frequency regions at the sensor locations. Second, even when these errors are larger, the time-fractional method performs better than the fractional-Laplacian method.

C. Spatially varying power-law absorption

One advantage of the time-fractional approach is that, unlike the fractional-Laplacian, the derivative is local in space. Heterogeneities typically manifest in three forms within biological media, the ambient density ρ_0 , the sound speed c_0 , and the absorption α . The variation in ρ_0 , which manifests as $\mathbf{u} \cdot \nabla \rho_0$ within the conservation of mass equation, can be removed, reducing the equations back to the homogeneous form, by considering ρ not as the true density but as the adjusted parameter described by $\rho - \mathbf{d} \cdot \nabla \rho_0$, where \mathbf{d} is the particle displacement. As such, the acoustic density fluctuation is not computed directly. There is, in addition, an adjusted loss term; however, the difference is

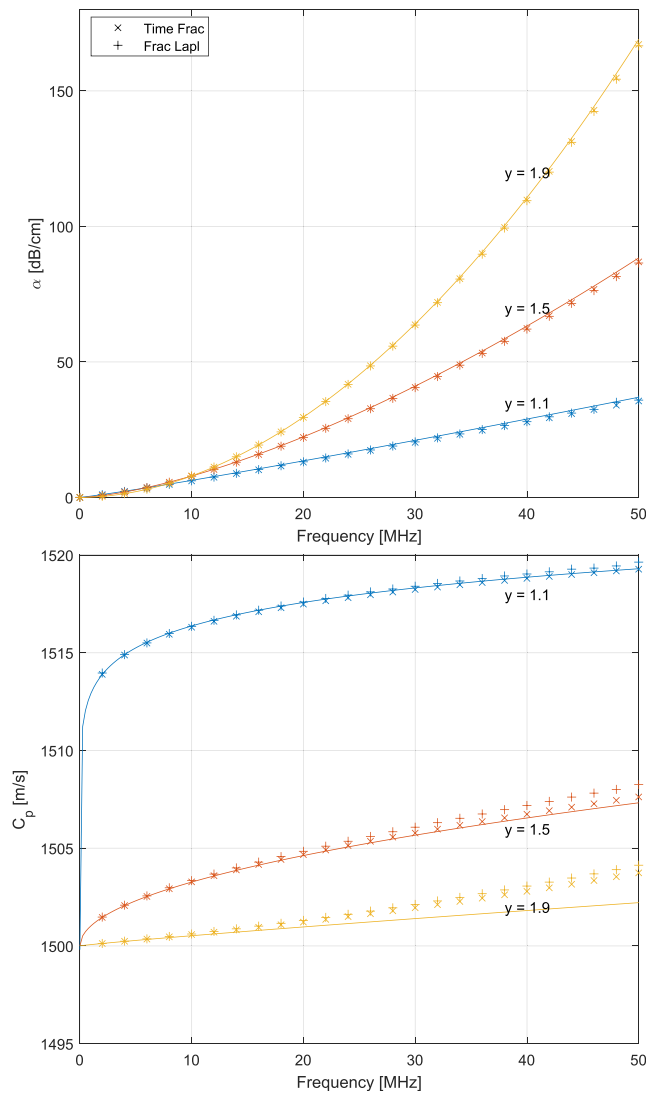


FIG. 7. As shown in Figs. 5 (top) and 6 (bottom), plotting the alpha for both the time-fractional derivative (\times) with $L = 120$, and with the fractional-Laplacian ($+$).

small in the majority of cases, and zero where $\nabla \rho_0 = 0$, and therefore may be neglected in the majority of cases. A varied c_0 is only observed in the computation of the equation of state, appearing both in the pre-factor, and within the loss term.

It is not common numerically to account for a varied absorption, despite being known to influence the final result within applications. For the time-fractional method, since each location in the domain is treated locally in the equation of state, we need only pre-compute the A_j and s_j [Eq. (10c)] parameters for each location, proceeding exactly as before, with increased storage, but no increased computational cost for each time step.

In Figs. 8 and 9, a system with varied absorption is illustrated. We have considered a 1D, 18.8 mm domain with 2048 grid points. A point source is located at 4.7 mm from the left edge of the domain. Sensors have been placed 5.2, 6.2, 8.2, 9.2, 11.1, and 12.1 mm to the right of the point source. We have then enforced that the absorption is defined

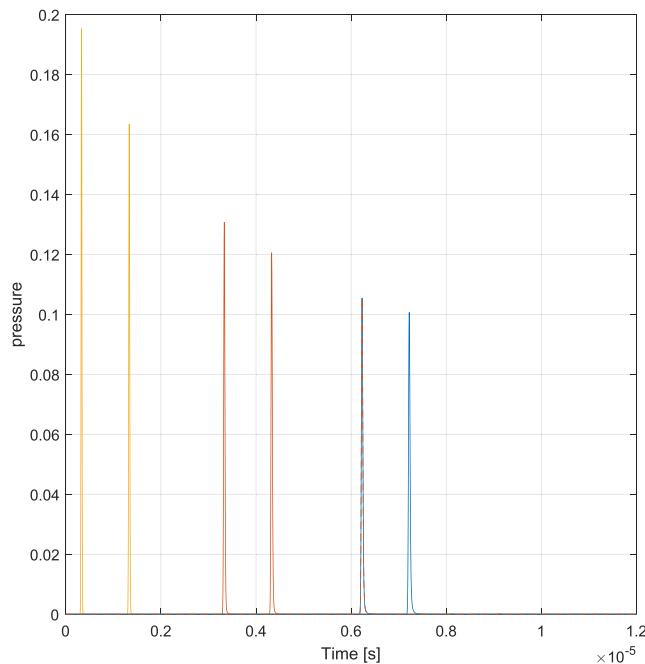


FIG. 8. Plot of the pressure at each time for each of the six sensors, with colours indicating the region of absorption in which they are located. Yellow plots correspond to $\alpha_0 = 0.25$ and $y = 1.9$ as between sensors one and two. Red plots correspond to $\alpha_0 = 0.125$ and $y = 1.5$, as used between sensors three and five. Blue plots use $\alpha_0 = 0.25$, $y = 1.1$, as for sensors five and six. Note that sensor five is located on the border between two regions.

by $\alpha = 0.05\omega^{1.9}$ between 0 and 7.2 mm from the left edge of the domain, and $\alpha = 0.125\omega^{1.5}$ between 7.2 and 11.1 mm. Finally, $\alpha = 0.25\omega^{1.1}$ from 11.1 mm to the rightmost edge of the domain. This locates the first two sensors within the first region, the third and fourth sensors in the second region, and finally, the sixth sensor in the third region. The fifth sensor is located exactly at the interchange between the second and third region of the domain. It should be noted that the α_0 values used here are half of the values given in Table I. This reduces the absorption effects and reflections as the wave changes between the regions and as a result, the numerical errors introduced in the calculation of α and c_p from the numerical data.

In Fig. 8, the sensor data from each of the six sensors can be observed, with colours indicating in which region of the domain they are located. These are then translated into plots of the absorption and the dispersion in Fig. 9 where matching colours have been used to indicate the regions for comparisons against the actual absorption and the Kramers–Kronig relation indicated once again with solid lines.

In Fig. 9, there is a region in which an error can be observed unlike those observed in Figs. 5 and 7. For $\omega < 10$ MHz for $y = 1.5$, observed more clearly in the plot of the dispersive sound speed, the Kramers–Kronig relation is poorly predicted. This is a result of a reflected wave being produced due to the change in absorption, since these propagate in the opposite direction to the initial wave, despite their small amplitude. This same error occurs in the first region, $y = 1.9$; however, it is less noticeable.

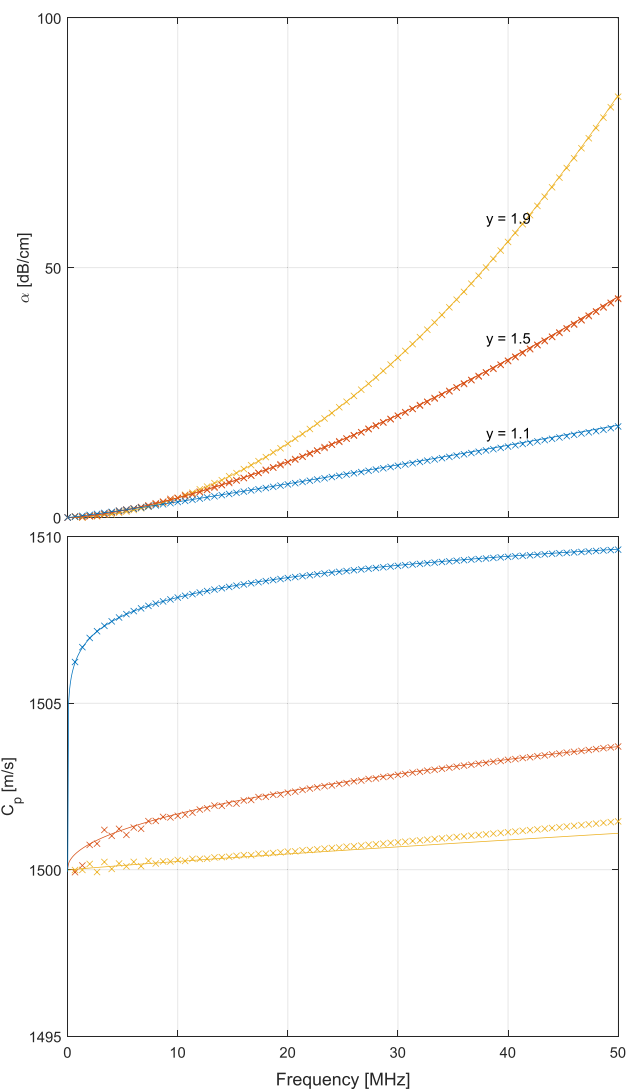


FIG. 9. As shown in Fig. 7, plotting α and dispersion from the time-fractional derivative with $L = 100$, with absorption plotted between sensors; one and two, three and four, four and five, and five and six. Yellow plots correspond to $\alpha_0 = 0.05$ and $y = 1.9$ as between sensors one and two. Red plots correspond to $\alpha_0 = 0.125$ and $y = 1.5$, as used between sensors three and five. Blue plots use $\alpha_0 = 0.25$, $y = 1.1$, as for sensors five and six.

It is additionally possible to model a varied absorption in both 2D and 3D; with Fig. 10, this is illustrated for a 3D example. We make use of a 3D Breast Phantom provided alongside Lou *et al.* (2017). In the breast phantom, we have modelled the different tissue types with different sound speeds and densities. In addition, we have then applied a varied absorption, according to the tissue type when running the simulation with the time-fractional method, or a uniform absorption for a loss described by the fractional-Laplacian. Sensors were located on the “outside” of the breast such that only the effects of the breast material properties are observed with a source represented by a single pulse from each voxel representing blood vessels at time, $t = 0$.

From Fig. 10, it can be observed that while both simulations produce similar signals, as time progresses, the arrival of the signals gradually vary an increased amount, while from

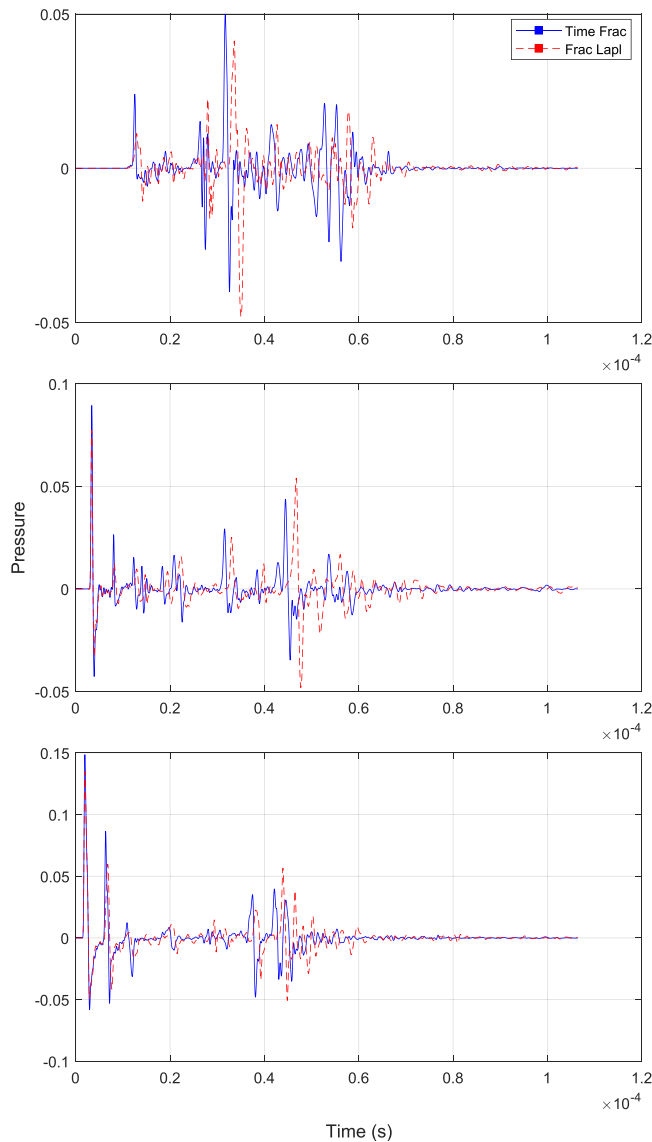


FIG. 10. Plots of three sensor data of the pressure at locations outside the breast. Plotted: (Red) homogeneous absorption with the fractional-Laplacian method. (Blue) Heterogeneous absorption with the time-fractional method.

even the first arrival time, the amplitudes of the waves are different. Which signal is greater, however, is not consistent with time. This variation between the signal with greater amplitude highlights that the two signals are decaying at different rates. While it should be noted that the homogeneous case would illustrate some additional errors, since the same CFL has been used for both simulations and the homogeneous cases use the *k*-Wave toolbox with the fractional-Laplacian loss, which was seen to have greater error in Fig. 4. It is clear that the differences between the two signals are mostly produced by the difference in the absorption, while the absorption used in the homogeneous case is chosen to match the absorption observed in most of the domain. As such, the waves will travel through regions with both higher and lower absorption with earlier arriving waves mainly travelling through the skin, and the latter travelling through more regions of fat, which has a lower absorption power-law exponent.

IV. DISCUSSION

The time-fractional static memory approach to the Caputo time-fractional derivative given in this paper has been previously detailed by Gutleb and Carrillo (2023) where it was compared against a variety of model problems in order to illustrate the effectiveness of the method. In their work, the fractional time derivative was applied to a second order differential equation for acoustic loss, although this is not the same acoustic loss as used in this work, even when transformed into the second order equations. Further distinguishing the works is the approach taken to the spatial dimensions, with the work here applying the time-fractional derivative on a uniform spatial grid. This may be considered a loss in problem generality; however, it allows the method to be more directly compared to the aforementioned numerical implementations of the fractional-Laplacian while also allowing easy treatment of the spatial domain.

The Caputo fractional derivative is defined by an integral over the full problem history. In order to avoid having to store the problem history within the numerical implementation, as is used for the static memory and logarithmic memory principles, here the problem history is stored in an iteratively defined $\phi_p(t)$, which when approximated numerically only requires a single time step of the problem history. Storing the problem history in this way does introduce a second integral on $(0, \infty)$ for which a quadrature rule has been applied with variables relating to the j th quadrature point indicated with a subscript j , with the total number of quadrature points denoted L , which is free to be chosen within the implementation of the method.

For a fixed value of L and computational grid of size N_X , the resulting method for approximating the fractional derivative requires a fixed memory cost, which is why this method is referred to as a static memory method. Applying the fractional time derivative to compute the loss operator only requires the additional storage of $L(N_X + 2) + N_X$ scalar variables compared to the memory requirements of the *k*-Wave toolbox, having changed only the method for computing the loss. This is a large memory requirement, particularly for 3D computational grids, given that L would typically be chosen between 80 and 120 in order to have likely observed convergence in L such that the remaining error comes from the time step (see Figs. 2 and 3). It is noted, however, that for many problems, the total number of time steps to be taken would be much larger than L , and storing the whole problem memory would require $n \times (N_X + 1)$ variables after n time steps.

The alternative “short term memory” and “logarithmic memory” principles choose which points of the problem history to be stored reducing this cost; however, both require a long history, increasing memory requirements, or lose accuracy as the total number of time steps increases. Of these methods, the logarithmic memory principle is more accurate for the same computational cost, while the fixed memory principle is as good or more accurate for a fixed length of history being considered.

In light of this, it is worth considering current high-performance computing trends where it may be observed that systems continue to evolve to address memory-bound applications. As such, methods like the one presented here may become increasingly attractive for large-scale acoustic simulations. The time-fractional approach presented here offers potential performance benefits for certain computing architectures, despite its increased memory requirements, compared to the fractional-Laplacian method. While the additional memory usage may be problematic for compute-bound systems, like graphics processing units it is well-suited for emerging central processing unit (CPU) designs optimized for memory-intensive workloads. For example, the NVIDIA Grace CPU Superchip (Nvidia, Santa Clara, CA) provides up to 960 GB of high-bandwidth LPDDR5X (Samsung Electronics, Suwon-si, South Korea) memory, making it capable of handling the increased memory footprint of this method. Additionally, by eliminating the need for the additional FFT operations per time step, this approach reduces computational complexity, which could lead to improved performance on memory-bound systems, particularly for the varied absorption case.

In works, such as [Chen and Holm \(2004\)](#), it is suggested that the fractional-Laplacian lends itself more directly to modelling variation in the spatial dimensions, being physically more valid. However, since the operator is derived globally by spatial Fourier transforms, local changes to the operator are not easy to account for, as such, the *k*-Wave toolbox only allows for a single power-law absorption. Using a time-fractional loss allows spatial changes in the derivative to not impact the computation, since each location has the corresponding fractional time derivative computed locally. This results in the additional computational cost of the method being reduced to the pre-computation of the s_j and A_j values for each value of y , with the trade-off being that the memory requirement is increased to $(3L + 1)N_X$. In cases where the spatial grid is large and only a few values of y are being considered, it would be possible to reduce the storage to $L(N_X + 2Y) + N_X$, where Y is now the number of different power-laws. However, this would have the increased computational cost of Y sums over j of A_j/ψ_j . These methods were used in the generation of Figs. 9 and 10, respectively. Considerations between which approach to use for a varied absorption power would include both storage and computation considerations, particularly if smoothing was performed on y across the domain. In order to generate Fig. 10, the computational time for the homogeneous case was approximately five times lower than that for the heterogeneous case.

In addition to the memory requirement and the observed computational time when comparing between loss computed with the fractional-Laplacian and the time-fractional methods for the loss, also of importance is the accuracy. In Fig. 4, it is observable that the time-fractional method produced significantly lower orders of magnitude of error than that of the fractional-Laplacian loss for the same size of time step,

particularly for values of y close to 1. It is possible that as a result of this, for such values, a time step that is two to four times larger could be utilised producing the same error for the absorption. It has not been investigated whether this difference in time stepping could suitably account for the computational differences.

V. CONCLUSION

The method for computation of the Caputo time-fractional derivative as described ([Birk and Song, 2010](#)) has been coded and applied to modelling power-law absorption within the first order wave equations as equivalent to the second order equation given by Caputo/Wismar [Eq. (1)]. It has been verified that the method performs as good or better at predicting the power-law absorption and dispersive sound speeds as the methods describing the loss by the fractional-Laplacian method for the same size of time step under a suitably chosen L , which describes the number of Gauss–Jacobi quadrature points used.

The method has then been applied to allow for varied power-law absorption, which has not previously been detailed within the literature. This is despite varied absorption being physically relevant to applications, including for ultrasound absorption, as the wave propagates through different tissue.

Further work on this topic would include further optimisations to the formulations for A_j , s_j , and $\phi_j(t)$, including lookup tables for the first two. It is, however, of note that the accurate calculation of the A_j and s_j is paramount to the method working, with higher point precision being required in the pre-computations performed in the time-fractional approach in order to retrieve an accurate approximation of the time-fractional derivative.

Additionally, it is possible that alternative choices of the quadrature rule for approximating the first order derivative, $\partial\rho/\partial t$, within the computation of ϕ_j may allow for even larger time steps, and exact forms of ϕ_j are given within the supplementary material. However, preliminary tests of these methods have not yielded the expected improvements but performed worse, even on model problems. This is possibly due to cancellation errors for the small time steps, such as the ones used on a fine grid; this would additionally raise the storage requirement of the problem.

It is possible that this method could be applied to other problems with fractional derivatives outside of the range $1 < y < 2$, as already detailed in [Birk and Song \(2010\)](#), with only small changes being made to the specific loss term in use.

Finally, comparisons could be made directly to existing methods for evaluation of the time-fractional derivative on the same model equation with spacial variations, such as the short term memory principle ([Podlubny, 1998](#)), the logarithmic memory principle ([Ford and Simpson, 2001](#)), and an approximate method for the equivalent Green's function solution ([Kelly and McGough, 2016](#)).

SUPPLEMENTARY MATERIAL

See the supplementary material for breakdowns of the mathematical formulations for τ , the rewriting of the fractional derivative, and integral evaluation under interpolation.

ACKNOWLEDGMENTS

This research was supported by the Engineering and Physical Sciences Research Council (EPSRC) under Grant Nos. EP/W029324/1, EP/T022280/1, and EP/T014369/1. We offer thanks to Dr. Jiří Jaroš for his insights on the computational trends.

AUTHOR DECLARATIONS

Conflict of Interest

The authors have no conflicts to disclose.

DATA AVAILABILITY

Data sharing is not applicable to this article as no new data were created or analyzed in this study.

¹In order to make the comparisons between the numerical methods applied for the computation of the time-fractional loss given here, and for the fractional-Laplacian method, which is implemented in the *k*-Wave toolbox (Treeby and Cox, 2010a). The code used to evaluate the problem numerically is identical to that in the *k*-Wave, except for the treatment of the loss.

²All of the numerical results presented in this paper have been produced using an adjusted version of the *k*-wave toolbox in MATLAB and is available at <https://github.com/MatthewJohnKing/k-wave-Time-Frac-Static-Memory.git>.

- Birk, C., and Song, C. (2010). "An improved non-classical method for the solution of fractional differential equations," *Comput. Mech.* **46**, 721–734.
- Blackstock, D. T. (1967). "Transient solution for sound radiated into a viscous fluid," *J. Acoust. Soc. Am.* **41**(5), 1312–1319.
- Caputo, M. (1966). "Linear models of dissipation whose q is almost frequency independent," *Ann. Geophys.* **19**(4), 383–393.
- Caputo, M. (1967). "Linear models of dissipation whose q is almost frequency independent—II," *Geophys. J. Int.* **13**(5), 529–539.
- Chen, W., and Holm, S. (2003). "Physical interpretation of fractional diffusion-wave equation via lossy media obeying frequency power law," *arXiv:math-ph/0303040*.
- Chen, W., and Holm, S. (2004). "Fractional Laplacian time-space models for linear and nonlinear lossy media exhibiting arbitrary frequency power-law dependency," *J. Acoust. Soc. Am.* **115**(4), 1424–1430.
- Courant, R., Friedrichs, K., and Lewy, H. (1967). "On the partial difference equations of mathematical physics," *IBM J. Res. Dev.* **11**(2), 215–234.
- Diethelm, K. (2008). "An investigation of some nonclassical methods for the numerical approximation of Caputo-type fractional derivatives," *Numer. Algor.* **47**(4), 361–390.
- Ford, N. J., and Simpson, A. C. (2001). "The numerical solution of fractional differential equations: Speed versus accuracy," *Numer. Algorithms* **26**, 333–346.
- Goss, S., Frizzell, L., and Dunn, F. (1979). "Ultrasonic absorption and attenuation in mammalian tissues," *Ultrasound Med. Biol.* **5**(2), 181–186.

- Gutleb, T. S., and Carrillo, J. A. (2023). "A static memory sparse spectral method for time-fractional PDEs," *J. Comput. Phys.* **494**, 112522.
- Kelly, J. F., and McGough, R. J. (2016). "Approximate analytical time-domain Green's functions for the Caputo fractional wave equation," *J. Acoust. Soc. Am.* **140**(2), 1039–1047.
- Li, F., Villa, U., Park, S., and Anastasio, M. A. (2022). "3-D stochastic numerical breast phantoms for enabling virtual imaging trials of ultrasound computed tomography," *IEEE Trans. Ultrason. Ferroelectr. Freq. Control* **69**(1), 135–146.
- Liebler, M., Ginter, S., Dreyer, T., and Riedlinger, R. E. (2004). "Full wave modeling of therapeutic ultrasound: Efficient time-domain implementation of the frequency power-law attenuation," *J. Acoust. Soc. Am.* **116**(5), 2742–2750.
- Lou, Y., Zhou, W., Matthews, T. P., Appleton, C. M., and Anastasio, M. A. (2017). "Generation of anatomically realistic numerical phantoms for photoacoustic and ultrasonic breast imaging," *J. Biomed. Opt.* **22**(4), 041015.
- Mainardi, F. (2022). *Fractional Calculus and Waves in Linear Viscoelasticity: An Introduction to Mathematical Models*, 2nd ed. (World Scientific, Singapore).
- Moran, C., Bush, N., and Bamber, J. (1995). "Ultrasonic propagation properties of excised human skin," *Ultrasound Med. Biol.* **21**(9), 1177–1190.
- Narayana, P. A., and Ophir, J. (1983). "On the frequency dependence of attenuation in normal and fatty liver," *IEEE Trans. Son. Ultrason.* **30**(6), 379–382.
- Podlubny, I. (1998). *Fractional Differential Equations: An Introduction to Fractional Derivatives, Fractional Differential Equations, to Methods of Their Solution and Some of Their Applications*, Mathematics in Science and Engineering Vol. 198 (Elsevier, Amsterdam, Netherlands).
- Stokes, G. G. (2007). "On the theories of the internal friction of fluids in motion, and of the equilibrium and motion of elastic solids," in *Classics of Elastic Wave Theory* (Society of Exploration Geophysicists, Houston, TX).
- Szabo, T. L. (1994). "Time domain wave equations for lossy media obeying a frequency power law," *J. Acoust. Soc. Am.* **96**(1), 491–500.
- Szabo, T. L. (2014). *Diagnostic Ultrasound Imaging: Inside Out* (Academic Press, Cambridge, MA).
- Tabei, M., Mast, T. D., and Waag, R. C. (2002). "A *k*-space method for coupled first-order acoustic propagation equations," *J. Acoust. Soc. Am.* **111**(1), 53–63.
- Treeby, B. E., and Cox, B. (2011). "A *k*-space Green's function solution for acoustic initial value problems in homogeneous media with power law absorption," *J. Acoust. Soc. Am.* **129**(6), 3652–3660.
- Treeby, B. E., and Cox, B. T. (2010a). "k-wave: MATLAB toolbox for the simulation and reconstruction of photoacoustic wave fields," *J. Biomed. Opt.* **15**(2), 021314.
- Treeby, B. E., and Cox, B. T. (2010b). "Modeling power law absorption and dispersion for acoustic propagation using the fractional laplacian," *J. Acoust. Soc. Am.* **127**(5), 2741–2748.
- Waters, K. R., Hughes, M. S., Mobley, J., Brandenburger, G. H., and Miller, J. G. (2000). "On the applicability of Kramers–Krönig relations for ultrasonic attenuation obeying a frequency power law," *J. Acoust. Soc. Am.* **108**(2), 556–563.
- Waters, K. R., Mobley, J., and Miller, J. G. (2005). "Causality-imposed (Kramers–Kronig) relationships between attenuation and dispersion," *IEEE Trans. Ultrason. Ferroelectr. Freq. Control* **52**(5), 822–823.
- Wells, P. (1975). "Absorption and dispersion of ultrasound in biological tissue," *Ultrasound Med. Biol.* **1**(4), 369–376.
- Wismer, M. G. (2006). "Finite element analysis of broadband acoustic pulses through inhomogeneous media with power law attenuation," *J. Acoust. Soc. Am.* **120**(6), 3493–3502.
- Yuan, L., and Agrawal, O. P. (2002). "A numerical scheme for dynamic systems containing fractional derivatives," *J. Vib. Acoust.* **124**(2), 321–324.